Preprints of the 19th World Congress
The International Federation of Automatic Control
Cape Town, South Africa. August 24-29, 2014

Energy Storage Requirements for Near-Optimal Reactive Control of a Wave Energy Device ⋆

Umesh A. Korde *

* *South Dakota School of Mines and Technology, Rapid City, SD 57701 USA (Tel: 1 (605) 355-3731; E-mail: Umesh.Korde@sdsmt.edu).*

Abstract: This paper investigates an approach to near-optimal real-time reactive control of wave energy devices based on time-domain up-wave surface elevation information. The paper first presents the overall approach required for such control, and recalls the need for future force and response information due to the causality of the radiation force and the non-causality of the exciting force (in relation to the wave profile at device centroid). The present approach is a realistic approximation based on linearized wave propagation and device dynamics models. For a predominantly heaving submerged point absorber in an approximately uni-directional incident wave field, the amount of instantaneous reactive power is compared with the instantaneous absorbed power. Although the net reactive energy is zero in the absence of actuator losses, the instantaneous reactive energy requirement for small devices in swell-dominated spectra may be significant. The time-domain calculations here confirm this and show that substantial amounts of energy may need to be exchanged with an external energy storage unit or the grid until sufficient energy has been absorbed.

1. INTRODUCTION

Active control of the hydrodynamic response of wave energy converters can enable over 2–5 fold increase in the overall efficiency depending on the device (Salter [1993], Eidsmoen [1996], Hansen and Kramer [2011], Korde [2014], (i) allowing fewer, structurally efficient smaller units to meet the required power generation targets, and (ii) improving the overall annual productivity of the device. For many devices, the economic benefits thus resulting may significantly offset the added expense of providing control.

It was shown some decades ago that, hydrodynamic control for greatest energy conversion efficiency ("optimal") in irregular waves requires future oscillation/exiting force information (Naito and Nakamura [1985], Falnes [1995]). Compromise solutions using velocity estimation based on time-series analysis of past velocities were reported some years ago (Korde [1999], Korde et al. [2002]).

A non-reactive time-domain switching control approach ('latching', later extended to declutching/clutching) using coordinated real-time application of intermittent braking forces was first tested in the seventies (Budal and Falnes [1980]) and then later studied by many authors (Hoskin et al. [1985], Falcao and Justino [1999], Perdigao and Sarmento [1989], Babarit and Clement [2006], Korde [2001], etc). The use of a high-pressure hydraulic power take-off was studied for a heaving buoy type device to optimize the converted hydraulic power in the time domain (Falcao [2008]). For a small, tubular oscillating water column device, a 'non-predictive' phase control strategy was also considered (Lopes et al. [2009]), with the understanding that the radiation impedance was small. Frequency domain 'complex-conjugate control' approaches comprising adjustable reactive loading for selective tuning to changing wave spectra have been studied since the mid-seventies (Salter [1978], Nebel [1992], Korde [1991]), etc. Such an approach was tested recently on the Wavestar device in Denmark (Hansen and Kramer [2011]).

A coupled fuzzy logic–robust controller was used recently for short term tuning with incoming-wave prediction in Schoen et al. [2011]. Some recently proposed time-domain control approaches were evaluated in Hals et al. [2011b]. A stochastic control approach based on past information only was recently investigated and found to produce good performance relative to optimal time-domain control (Scruggs et al. [2013]). Constrained optimal control under 'hard' displacement and force constraints on the primary converter was reported recently in (Hals et al. [2011a], Bacelli and Ringwood [2013]). The effect of device geometry on the 'prediction horizon' for real-time control was studied with a view to velocity/exciting force prediction (Fusco and Ringwood [2012]), and a technique for short-term wave forecasting for use in real-time control was examined in Fusco and Ringwood [2010].

The research underlying the present paper is based on hydrodynamics-driven modeling of wave propagation and device response and known results (Naito and Nakamura [1985], Falnes [1995], Korde [2014]). Further, it is noted that over distances approaching 1–2 km, a deterministic linear-system type understanding of wave propagation may be valid for primarily uni-directional waves (Belmont et al. [2006], Dannenberg et al. [2010]), etc. X-band radar technology has been used in recent years for real-time prediction of ship motions using wave profile measurements

⋆ I thank Larry and Linda Pearson for their support through the Pearson endowment.

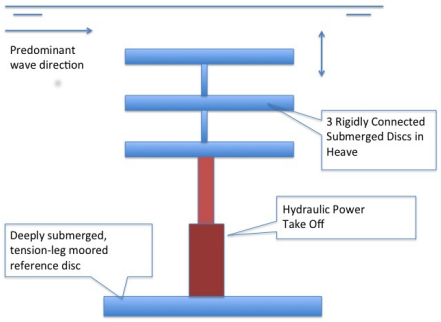

Fig. 1. Schematic view of the device being investigated here.

500–1500 m in the up-wave direction (Dannenberg et al. [2010]) and could be employed in the present application.

For greater insight, a predominantly heaving point absorber is used in this work. As Figure 1 shows, the primary energy converter is comprised of three submerged discs on a vertical axis. Secondary conversion is by means of a double-acting hydraulic cylinder which is also used for control. A deeply submerged disc provides a reference for energy conversion. Earlier work showed that the exciting force and radiation damping functions become flatter in the frequency domain with submergence depth, leading to narrower impulse response functions in the time domain (Korde and Ertekin [2013]). This in turn enables shorter up-wave distances for wave profile measurement (Korde [2014]). However, radiation damping decreases with submergence depth while the frequency-independent reactive terms such as rest mass and stiffness remain constant. Thus, though large reactive forces are probably to be expected for most small point absorbers operating in swell-rich wave climates, these are likely to pose a greater challenge for submerged point absorbers. Implications of this situation are studied here, and it is found that the device must draw from and pump into (i) initially the grid or another device, and (ii) later an on-board energy storage system.

2. REAL TIME NEAR-OPTIMAL CONTROL USING UP-WAVE SURFACE ELEVATION

For the three-disc body in predominant heave and operating in primarily uni-directional irregular waves propagating from left to right along the positive x axis, the linear equation of motion is (Falnes [1995]),

$$[m+\mu(\infty)]\,\dot{v}+c_d v+\int_0^\infty h_r(\tau)v(t-\tau)d\tau + k_h\int_{-\infty}^{t} v(\tau)d\tau = F_f+F_r \qquad (1)$$

Here m is the in-air mass of the 3-disc body, $\mu(\infty)$ the infinite-frequency added mass in heave, k_h is the steady stiffness in the hydraulic power take-off, c_d the constant damping in the system to approximate viscous losses, and $h_r(t)$ the radiation [without the contribution of $\mu(\infty)$]impulse response kernel. The goal is to apply an instantaneous control force $F_r(t)$ such that the resulting heave velocity $v(t)$ is synchronous with the exciting force $F_f(t)$ in heave due to the diffraction wave field produced when the body is held fixed. The radiation force is expressed by the convolution term on the left and is affected by the wave field created by body oscillation in calm water until a time far enough back into the past. Both the exciting force and the radiation force in heave act at the body centroid.

2.1 Causality of the radiation impulse response function

The radiation impulse response function/kernel $h_r(t)$ is causal in that only the past and current velocity affects the current radiation force. In other words, $h_r(t)=0, t<0$. This implies that its Fourier transform $H_r(i\omega)$ is analytic in the upper half of the complex-frequency plane (Wehausesn [1992]). Further, since $h_r(t)$ is real-valued (velocity and radiation force being real-valued), $H_r(-i\omega)=H_r^*(i\omega)$. With

$$\int_{-\infty}^{\infty} h_r(t)\mathrm{e}^{-i\omega t}dt = H_r(i\omega)=\lambda(\omega)+i\omega\mu(\omega) \qquad (2)$$

where $\lambda(\omega)$ and $\mu(\omega)$ are the frequency-dependent radiation damping and added mass respectively. Since $H_r(-i\omega)=H_r^*(i\omega)$, $\lambda(\omega)$ is an even function and $\omega\mu(\omega)$ is an odd function. Further, since both $\lambda(\omega)$ and $\mu(\omega)\to 0$ as $\omega\to\infty$, it can be shown that, for a real-valued ω,

$$PV\int_{-\infty}^{\infty}\frac{H_r(i\varpi)}{\varpi-\omega}d\varpi=\pi i H_r(i\omega) \qquad (3)$$

which implies that

$$\lambda(\omega)=\frac{1}{\pi}PV\int_{-\infty}^{\infty}\frac{\varpi\mu(\varpi)}{\varpi-\omega}d\varpi$$
$$\omega\mu(\omega)=-\frac{1}{\pi}PV\int_{-\infty}^{\infty}\frac{\lambda(\varpi)}{\varpi-\omega}d\varpi \qquad (4)$$

where PV denotes principal value. Equation (4) shows the Kramers–Kronig relations (Jeffreys [1984]). $\lambda(\omega)$ and $\mu(\omega)$ are thus related to each other, with

$$\lambda(\omega)=\int_0^\infty h_r(t)\cos\omega t dt$$
$$\mu(\omega)=-\frac{1}{\omega}\int_0^\infty h_r(t)\sin\omega t dt \qquad (5)$$

2.2 Non-causality of the exciting force impulse response function

In the frequency domain the exciting force is typically defined per unit incident wave amplitude at the body centroid. Inverse Fourier transformation based on this approach leads to a convolution of an exciting force impulse response function with the incident wave surface elevation at the centroid location. For most geometries including the present, this impulse response function is non-causal, given that (i) the force is in fact distributed over a surface, and (ii) the force begins to act even as the incident waves are approaching the device (cf. Falnes [1995]). In terms of the wave elevation at the centroid x_B,

$$F_f(t)=\int_{-\infty}^{\infty}h_f(\tau)\eta(x_B;t-\tau)d\tau \qquad (6)$$

where $h_f(t)$ is the impulse response kernel for exciting force, $\eta(x_B;t)$ is the wave surface elevation at point x_B and time t, and x_B the device location relative to origin.

$$\eta(x_B;t) = \frac{1}{2\pi}\int_{-\infty}^{\infty} \eta(x_B;i\omega)\mathrm{e}^{i\omega t}d\omega \tag{7}$$

with

$$\eta(x_B;i\omega) = A(i\omega)\mathrm{e}^{-ik(\omega)x_B} \tag{8}$$

so that, with $F_f(i\omega) = H_f(i\omega)\eta(x_B;i\omega)$,

$$h_f(t) = \frac{1}{2\pi}\int_{-\infty}^{\infty} H_f(i\omega)\mathrm{e}^{i\omega t}d\omega \tag{9}$$

For reasons (i) and (ii) above, $h_f(t)$ is non-causal, or $h_f(t) \neq 0$, $t < 0$.

2.3 Up-wave surface elevation

Full reactive control in the time domain (generalization of 'complex-conjugate' control) requires real-time cancellation of all reactive forces on the body and application of a damping force that in frequency domain would equal the force due $\lambda(\omega) + c_d$. The reactive force includes the component similarly related to $\omega\mu(\omega)$ in addition to the rest-mass and stiffness on the body. For full reactive control, the required $F_r(r)$ is

$$F_r(t) = [m + \mu(\infty)]\dot{v} + k_h\int_{-\infty}^{t} v(\tau)d\tau + F_c(t) \tag{10}$$

where the first two terms depend on just the instantaneous acceleration and deflection of the device and the physical parameters, and comprise the 'basic' reactive force. The 'added' force $F_c(t)$ is based on impulse response functions h_λ and h_μ defined as,

$$\begin{aligned} h_\lambda(t) &= \frac{1}{2\pi}\int_{-\infty}^{\infty} \lambda(\omega)\mathrm{e}^{i\omega t}d\omega \\ h_\mu(t) &= \frac{1}{2\pi}\int_{-\infty}^{\infty} i\omega\mu(\omega)\mathrm{e}^{i\omega t}d\omega \end{aligned} \tag{11}$$

with

$$F_c(t) = -c_d v(t) - \int_{-\infty}^{\infty} h_\lambda(\tau)v(t-\tau)d\tau + \int_{-\infty}^{\infty} h_\mu(\tau)v(t-\tau)d\tau \tag{12}$$

Application of force $F_r(t)$ given by (10) and (12) into equation (1) causes the device to oscillate at optimal velocity $v_{opt}(t)$ (as defined in Evans [1976], Falnes [1995]) given by

$$2\left(c_d + \int_{-\infty}^{\infty} h_\lambda(\tau)v_{opt}(t-\tau)d\tau\right) = F_f(t) \tag{13}$$

In practice, the tails of both h_r and h_f become small enough over time. Thus, $h_r(t)$, h_λ, and $h_\mu \to 0$ as $t \geq t_c$, and $h_f(t) \to 0$, for $t < -t_{f1}$ and $t > t_{f2}$. Letting $t_f = \max[t_{f1}, t_{f2}]$,

$$\begin{aligned} 2\left(c_d + \int_{-t_c}^{t_c} h_\lambda(\tau)v_o(t-\tau)d\tau\right) &= F_f(t) \\ = \int_{-t_f}^{t_f} h_f(\tau)\eta(x_B;t-\tau)d\tau \end{aligned} \tag{14}$$

where now $v(t)$ is replaced by $v_o(t)$, which is the device velocity under near-optimal control as enabled by $F_r(t)$ based on the approximate $F_c(t)$.

To synthesize $F_c(t)$ therefore, estimates of velocity up to $t = t_c$ into the future are required. If the force F_f is used in this estimation, then F_f estimates are required up to $t = t_f$ further into the future (i.e. up to $t = t_c + t_f$). For a predominantly uni-directional linear progressive wave field approaching the device, it is relatively straightforward to obtain these estimates, since in realistic situations, (i) incident wave spectral density $S(\omega) \to 0$, for $0 < \omega \leq \omega_l$, and (ii) the functions h_f and h_r become independent of water depth beyond a finite depth h (enabling a 'finite-depth approximation'). Thus, it is reasonable to define a maximum group velocity $v_{max} = \sqrt{gh}$ (Falnes [1995]), which equals the phase velocity for the fastest-traveling waves in the spectrum. With negligible loss of information, and one may then use v_{max} to 'map' t_f and t_c to positions along the x axis, which defines the wave propagation direction. Thus, right-shifted versions of h_f, h_λ, and h_μ can be defined as,

$$\begin{aligned} h_{f_d}(t) &= h_f(t - t_c) \\ h_{\lambda c}(t) &= h_\lambda(t - t_c) \\ h_{\mu c}(t) &= h_\mu(t - t_c) \end{aligned} \tag{15}$$

With $d = v_{max}t_f$, and $d_c = v_{max}t_c$, the frequency-domain equivalent relations to equation (15) are,

$$\begin{aligned} H_{fd}(i\omega) &= H_f(i\omega)\mathrm{e}^{-ik(\omega)d} \\ \lambda_c(i\omega) &= \lambda(\omega)\mathrm{e}^{-ik(\omega)d_c} \\ \mu_c(i\omega) &= \mu(\omega)\mathrm{e}^{-ik(\omega)d_c} \end{aligned} \tag{16}$$

where $-i\omega t_f$ and $-i\omega t_c$ have been replaced by $-ik(\omega)d$ and $-ik(\omega)d_c$ respectively. Now, ignoring any viscous attenuation effects, if x_A is a point to the left of, i.e. up-wave of x_B, so that $x_B - x_A = d$, then for the frequency ω and wave number $k(\omega)$,

$$\eta(x_A;i\omega) = \mathrm{e}^{ik(\omega)d}\eta(x_B;i\omega) \tag{17}$$

Similarly, for points $x_C = x_B - d_c$, and $x_R = x_B - d_R$, where $d_R = d + d_c$,

$$\begin{aligned} \eta(x_C;i\omega) &= \mathrm{e}^{ik(\omega)d_c}\eta(x_B;i\omega) \\ \eta(x_R;i\omega) &= \mathrm{e}^{ik(\omega)d_R}\eta(x_B;i\omega) \end{aligned} \tag{18}$$

Since the device response is linear, the velocity $v(i\omega)$ at x_B must be related as in equation (18) to the velocity v_C of a 'virtual device' placed a distance d_C up-wave at x_C, and

$$v_C(i\omega) = v(i\omega)\mathrm{e}^{ik(\omega)d_c} \tag{19}$$

It follows that,

$$\begin{aligned} &F_f(i\omega) = H_f(i\omega)\eta(x_B;i\omega) \approx H_{fd}(i\omega)\eta(x_A;i\omega) \\ &\lambda(\omega)v(i\omega) = \lambda_c(i\omega)v_C(i\omega), \quad \omega\mu(\omega)v(i\omega) = \omega\mu_c(i\omega)v_C(i\omega) \end{aligned} \tag{20}$$

This leads to the time-domain expression for the control force component $F_c(t)$,

$$\begin{aligned} F_c(t) = &-\left(c_d v_c(t) + \int_0^{2t_c} h_{\lambda c}(\tau)v_c(t-\tau)d\tau\right) \\ &+ \int_0^{2t_c} h_{\mu c}(\tau)v_c(t-\tau)d\tau \end{aligned} \tag{21}$$

where $v_c(t)$ is the velocity of a virtual device at x_C, to find which, the wave profile d further up-wave at $d_R = d_c + d$ is needed.

3. CONTROL FORCES, ABSORBED AND REACTIVE ENERGY

3.1 Resistive and reactive forces

In time-domain simulations and in experiments it is relatively straightforward to synthesize the basic reactive force

using displacement and acceleration measurements as

$$F_s(t) = [m + \mu(\infty)]\dot{v}(t) + k_h \int_{-\infty}^{t} v(\tau)d\tau \qquad (22)$$

The desired optimal velocity in the frequency domain $v_o(i\omega)$ can be expressed as

$$v_o(i\omega) = \frac{H_{fd}(i\omega)\eta(x_A; i\omega)}{2[c_d + \lambda(\omega)]} \qquad (23)$$

In the time domain,

$$v_o(t) = \int_0^t h_o(\tau)\eta(x_A; t-\tau)d\tau \qquad (24)$$

where

$$h_o(t) = \frac{1}{2\pi}\int_{-\infty}^{\infty} \frac{H_{fd}(i\omega)}{2[c_d + \lambda(\omega)]} \mathrm{e}^{i\omega t} d\omega \qquad (25)$$

With the control force $F_r(t)$ fully synthesized, the velocity $v(t) = v_{act}(t)$. Then, absent measurement and model errors and unmodeled disturbances (as in the present simulation), $v_{act}(t) = v_o(t)$ within numerical truncation errors. In practice, closed-loop control can be used to drive v_{act} closer to v_o with all of the forces F_s, F_l, and F_a in place. The damping or power-absorbing component F_l of the applied 'added' force can be found using the desired optimal velocity at x_C.

$$F_l(t) = -\int_0^{2t_R} h_{l1}(\tau)\eta(x_R; t-\tau)d\tau - \int_0^{2t_f} h_{l2}(\tau)\eta(x_A; t-\tau)d\tau \qquad (26)$$

where,

$$h_{l1}(t) = \frac{1}{2\pi}\int_{-\infty}^{\infty} \frac{\lambda_c(\omega)H_{fd}(i\omega)}{2[c_d + \lambda(\omega)]} \mathrm{e}^{i\omega t} d\omega$$
$$h_{l2}(t) = \frac{1}{2\pi}\int_{-\infty}^{\infty} \frac{c_d H_{fd}(i\omega)}{2[c_d + \lambda(\omega)]} \mathrm{e}^{i\omega t} d\omega \qquad (27)$$

The reactive part of the 'added' force is given by,

$$F_a(t) = \int_0^{2t_R} h_a(\tau)\eta(x_R; t-\tau)d\tau \qquad (28)$$

where

$$h_a(t) = \frac{1}{2\pi}\int_{-\infty}^{\infty} \frac{i\omega\mu_c(i\omega)H_{fd}(i\omega)}{2[c_d + \lambda(\omega)]} \mathrm{e}^{i\omega t} d\omega \qquad (29)$$

In practice, $\eta(x_A; t)$ and $\eta(x_R; t)$ can both be measured by radar or another sensor. In simulations, they can be computed for a given power spectrum $S(\omega)$ with $A(\omega) = \sqrt{S(\omega)/2}$ where $A(i\omega) = A(\omega)\mathrm{e}^{i\theta(\omega)}$ and $\theta(\omega)$ is a random number in the interval $[0,\ 2\pi]$. Then,

$$\eta(x_A; t) = \frac{1}{2\pi}\int_{-\infty}^{\infty} A(\omega)\mathrm{e}^{-i[k(\omega)x_A - \omega t + \theta(\omega)]} d\omega$$
$$\eta(x_R; t) = \frac{1}{2\pi}\int_{-\infty}^{\infty} A(\omega)\mathrm{e}^{-i[k(\omega)x_R - \omega t + \theta(\omega)]} d\omega \qquad (30)$$

3.2 Absorbed and reactive power and energy

Three powers are important to consider. The time-averaged incident power on disc diameter $2R$ supplied by the waves is

$$P_{inc} = 0.49 H_s^2 T_e(2R) \qquad (31)$$

The instantaneous power absorbed by the applied resistive force F_l is,

$$P_w(t) = \frac{1}{T}\int_0^T [F_l(t) + c_d v_{act}(t)]v_{act}(t)dt \qquad (32)$$

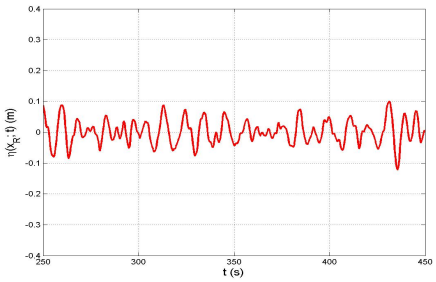

Fig. 2. Incident wave surface elevation 427 up-wave of the device.

where $v_{act}(t)$ is the device velocity with the forces $F_s(t)$, $F_l(t)$, and $F_a(t)$ applied. The instantaneous reactive power can be found as,

$$P_{reac}(t) = P_{cs}(t) + P_{ca}(t) \qquad (33)$$

with

$$P_{cs}(t) = \left\{[m + \mu(\infty)]\dot{v}_{act}(t) + k_h \int_{-\infty}^{t} v_{act}(\tau)d\tau\right\} v_{act}(t)$$
$$P_{ca}(t) = F_a(t)v_{act}(t) \qquad (34)$$

The cumulative energy at $t = T$ absorbed by the resistive force, that supplied and reclaimed by the reactive forces, and that supplied by incident waves can be found as,

$$E_{abs}(T) = \int_0^T P_w(t)dt$$
$$E_{reac}(T) = \int_0^T P_{reac}(t)dt$$
$$E_{inc}(T) = P_{inc}T \qquad (35)$$

For large enough T, $E_{reac}(T) \to 0$ when actuator losses are ignored, as in this work. When such losses are significant, a growing net loss of energy will be incurred over time. When $E_{abs}(T) > E_{reac}(T)$, the system can supply the necessary reactive power internally. However, while $E_{reac}(T) > E_{abs}(T)$, energy must be drawn from on-board storage (batteries, compressed air, etc.), other devices, or from the grid.

4. SIMULATIONS

Time domain calculations were performed for the present submerged 3-disc device with disc radius R of 1 m and disc vertical spacing of 1 m. Submergence depth of the topmost disc was 2 m, to prevent loss of static submergence up to wave amplitudes approaching 2 m. The hydraulic power take-off was assumed to be capable of generating the large control forces required in swell-dominated irregular waves. The exciting force and hydrodynamic coefficients in heave were computed as discussed in Korde [2014]. A disc thickness of 0.2 m was used for each disc, and a steady stiffness k_h =10 kN/m was used for the hydraulic power take-off. A value $h = 225$ m was used for the water depth.

5. DISCUSSION

The three impulse response functions h_{l1}, h_{l2}, and h_a are very nearly causal for the chosen t_f and t_c values (Korde [2014]). Calculations are carried out for the 2-parameter spectra over a range of energy periods and significant

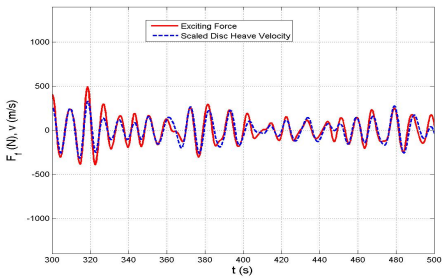

Fig. 3. Exciting force and heave velocity with present control approach.

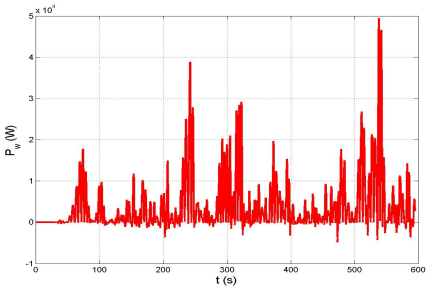

Fig. 4. Absorbed power as a function of time ($T_e = 11$s, $H_s = 1$ m).

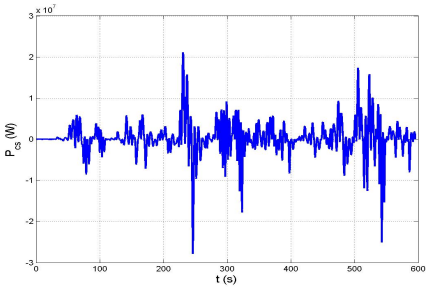

Fig. 5. Total reactive power P_{reac} as a function of time ($T_e = 11$s, $H_s = 1$ m).

wave heights. For $T_e = 11$ s and $H_s = 1$ m, the wave profile synthesized at $x_R = 427$ m is shown in Figure 2. The heave exciting force and device heave velocity under near-optimal control are shown in Figure 3. The velocity seems to be synchronous with the force for the most part, although small differences exist, which may have resulted from an incomplete synthesis of the terms used to compute v_{act} and errors in the inverse Fourier transformations. Figure 4 shows the absorbed power under near-optimal control over the calculation range. While the maximum approaches 40 kW, the average over 600 s is about 3.5 kW. Small amounts of power are returned due to slight errors in the velocity-force combination. This behavior was also noted in Naito and Nakamura [1985] and could arise at least in part from an incomplete synthesis of h_{l1} and h_{l2}, and in part due to errors in the inverse Fourier transformation.

Figure 5 plots the instantaneous reactive power needed to apply the reactive part $F_s(t) + F_a(t)$ of the control force. The instantaneous magnitudes are seen to be very high, although the average here must be zero within numerical

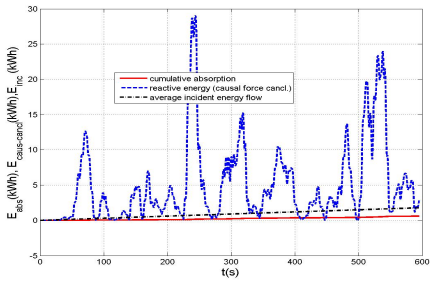

Fig. 6. Instantaneous total reactive energy E_{reac} requirement together with absorbed energy E_{abs} and incident energy E_{inc} as a function of time ($T_e = 11$s, $H_s = 1$ m).

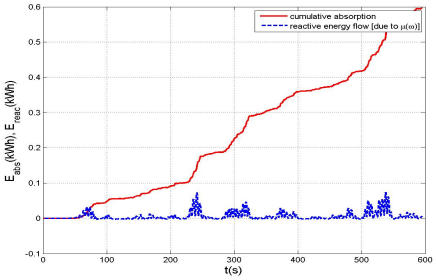

Fig. 7. Instantaneous reactive energy requirement for frequency-dependent added mass together with absorbed energy E_{abs} and incident energy E_{inc} as a function of time ($T_e = 11$s, $H_s = 1$ m).

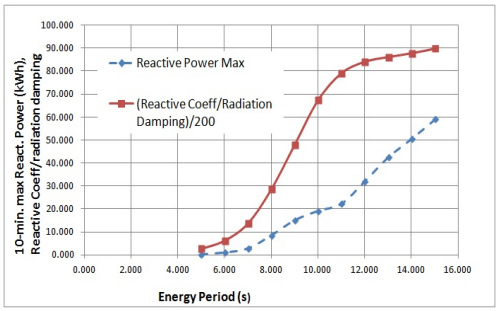

Fig. 8. Maximum total instantaneous reactive energy requirement, and the reactive/resistive term ratio as a function of time (over an range of energy periods T_e for $H_s = 1$ m).

errors. Note that the power lost in the actuator has been ignored here. However, large instantaneous power needs to be provided by the on-board machinery and any energy storage system. This point is examined further in the following results. Figures 6 and 7 compare the values E_{abs}, E_{reac} (for basic and added forces), and E_{inc} under the present near-optimal control over a 10-minute simulation for a spectrum with $H_s = 1$ m and $T_e = 11$s.

The instantaneous E_{reac} values are considerably greater than E_{abs} as well as E_{inc}. Although E_{abs} does increase with time, a simple extrapolation of the plot shows that several hours of near-optimal control operation is required before the device is able to store enough energy on-board for subsequent self-sufficient operation. The difference between the instantaneous energy requirement of the 'added'

reactive force component and the absorbed energy is of much less concern, as only a small amount of energy needs to be imported and only over the first few minutes. It is thus the 'basic' reactive component that requires large instantaneous energy. The near-optimal absorbed power is determined by the radiation damping, while the reactive power predominantly by the rest mass and stiffness in addition to the infinite-frequency added mass. The radiation damping decreases with submergence depth while the reactive terms are independent of submergence depth. Hence, the disparity between absorbed energy and maximum reactive energy values is likely be greater for submerged devices. This point could be important from an overall design standpoint. The increase in the reactive/resistive term ratio with wave period helps to explain the increase in the maximum instantaneous reactive energy amounts with energy period, as summarized in Figure 8.

6. CONCLUSION

A potentially important consideration relating to smooth real-time near optimal 'complex-conjugate' control of a submerged device was studied. The overall control approach was summarized, and principal time-domain simulation results were discussed. The energy absorbed over time was compared with the reactive energy that needs to flow through the primary converter and power take-off. Over a 10-minute period, the maximum instantaneous reactive energy was found to be considerably greater than the energy absorbed as of that instant. Until the device has generated sufficient energy to be able to replenish on-board or near-by energy storage units, the energy needs to be drawn from other devices or the grid. Even though the net absorption of this energy may be small for well-designed actuators, the large instantaneous amounts of reactive energy require attention at the design stage. The difference between maximum reactive energy and absorbed energy may be smaller for some floating devices, likely requiring less stored or imported energy.

REFERENCES

A. Babarit and A.H. Clement. Optimal latching control of a wave energy device in regular and irregular waves. *Applied Ocean Research*, 28(2):77–91, 2006.

G. Bacelli and J.V. Ringwood. A geometric tool for analysis of position and force constraints in wave energy converters. *Ocean Engineering*, 65, 2013.

M.R. Belmont, J.M.K. Horwood, R.W.F Thurley, and J. Baker. Filters for linear sea-wave prediction. *Ocean Engineering*, 33(17–18):2332–2351, 2006.

K. Budal and J. Falnes. Interacting point absorbers with controlled motion. In B.M. Count, editor, *Power from Sea Waves*, pages 381–399. Academic Press, London, 1980.

J. Dannenberg, P. Naaijen, K. Hessner, H. den Boom, and K. Reichert. The on board wave and motion estimator OWME. In *Proc. Int. Soc. Offshore and Polar Engr. Conf.*, 2010.

H. Eidsmoen. *On theory and simulation of heaving-buoy wave energy converters with control.* PhD thesis, Norwegian University of Science and Technology, Trondehim, Norway, 1996.

D.V. Evans. A theory for wave power absorption by oscillating bodies. *J. Fluid Mechanics*, 77(1):1–25, 1976.

A.F.O. Falcao. Phase control through load control of oscillating body wave energy converters with hydraulic PTO system. *Ocean Engineering*, 35:358–366, 2008.

A.F.O. Falcao and P.A.P. Justino. OWC wave energy devices with air flow control. *Ocean Engineering*, pages 1275–1295, 1999.

J. Falnes. On non-causal impulse response functions related to propagating water waves. *Applied Ocean Research*, 17(6):379–389, 1995.

F. Fusco and J.V. Ringwood. Short-term wave forecasting for real-time control of wave energy converters. *IEEE Trans. on Sustainable Energy*, 1(2):99–106, 2010.

F. Fusco and J.V. Ringwood. A study of the prediction requirements in real-time control of wave energy converters. *IEEE Transactions on Sustainable Energy*, 3(1):176–184, 2012.

J. Hals, J. Falnes, and T. Moan. Constrained optimal control of a heaving buoy wave energy converter. *J. Offshore Mechanics and Arctic Engineering*, 133(1):1–15, 2011a.

J. Hals, J. Falnes, and T. Moan. A comparison of selected strategies for adaptive control of wave energy converters. *J. Offshore Mechanics and Arctic Engineering*, 133(3):1–12, 2011b.

R.H. Hansen and M.M. Kramer. Modeling and control of the wave star prototype. In *Proc. 9th European Wave and Tidal Energy Conference*, 2011. Southampton, UK, paper 163.

R.E. Hoskin, B.M. Count, N.K. Nichols, and D.A.C. Nicol. Phase control for the oscillating water column. In D.V. Evans and A.F. O. Falcao, editors, *Proc. IUTAM Symp. Hydrodynamics of Wave Energy Utilization*, pages 257–268. Springer Verlag, Berlin, 1985.

E. R. Jeffreys. Simulation of wave power devices. *Applied Ocean Research*, 6(1):31–39, 1984.

U.A. Korde. A power take-off mechanism for maximizing the performance of an oscillating water column wave energy device. *Applied Ocean Research*, 13(2):75–81, 1991.

U.A. Korde. Efficient primary energy conversion in irregular waves. *Ocean Engineering*, 26:625–651, 1999.

U.A. Korde. Phase control of floating bodies from an on-board reference. *Applied Ocean Research*, 23:251–262, 2001.

U.A. Korde. On using up-wave surface elvation for efficient wave energy conversion in irregular waves. *Applied Ocean Research*, 2014. in press.

U.A. Korde and R.C. Ertekin. An open water submerged device for wave energy focusing and conversion. In *Proc. 10th European Wave and Tidal Energy Conference (EWTEC 2013)*, 2013. Aalborg, Denmark.

U.A. Korde, M.P. Schoen, and F. Lin. Strategies for time-domain control of wave energy devices in irregular waves. In *Proc. 11th Int. Soc. Offshore and Polar Engr. (ISOPE) Conference*, 2002. Stavanger, Norway.

M.F.P. Lopes, J. Hals, R.P.F. Gomes, T. Moan, L.M.C. Gato, and A.F.O. Falcao. Experimental and numerical investigation of non-predictive phase control strategies for a point absorbing wave energy converter. *Ocean Engineering*, 36:386–402, 2009.

S. Naito and S. Nakamura. Wave energy absorption in irregular waves by feedforward control system. In D.V. Evans and A.F. O. Falcao, editors, *Proc. IUTAM Symp. Hydrodynamics of Wave Energy Utilization*, pages 269–280. Springer Verlag, Berlin, 1985.

P. Nebel. Maximizing the efficiency of wave-energy plants using complex conjugate control. *Proc. IMechE Part I - Journal of Systems and Control Engineering*, 206(4):225–236, 1992.

J.N.B.A. Perdigao and A.J.N.A. Sarmento. A phase control strategy for OWC devices in irregular waves. In J. Grue, editor, *Proc. 4th Int. Workshop on Water Waves and Floating Bodies*, pages 205–209, 1989.

S.H. Salter. Development of the duck concept. In *Proc. Wave Energy Conference*, 1978. Heathrow, U.K.

S.H. Salter. Changing the 1981 spine-based ducks. In *Proc. 1st European Wave Energy Conf.*, 1993. Edinburgh, Scotland.

M.P. Schoen, J. Hals, and T. Moan. Wave prediction and robust control of heaving wave energy devices for irregular waves. *IEEE Trans. Energy Conversion*, 26(2):627–638, 2011.

J.T. Scruggs, S.M. Lattanzio, A.A. Taflanidis, and I.I. Cassidy. Optimal causal control of a wave energy converter in a random sea. *Applied Ocean Research*, 42:1–15, 2013.

J.V. Wehausesn. Causality and the radiation condition. *J. Engineering Mathematics*, 26:153–158, 1992.